On the Modeling and Design of Modular Multilevel Converters With Parametric and Model-Form Uncertainty Quantification

Niloofar Rashidi, *Member, IEEE*, Rolando Burgos, *Member, IEEE*, Chris Roy, and Dushan Boroyevich, *Fellow, IEEE*

***Abstract*—Modeling and design with parametric and model-form uncertainty quantification is an alternative to conventional model-based design approaches as it improves the existing modeling practice and validates the model used in the design of power converters. However, in the case of modular multilevel converters (MMCs), uncertainty quantification, as the main step in this design methodology, becomes challenging due to the inherent complexity and sheer size of such units. In this article, these limitations are discussed and a systematic study for developing a simplified testbed for uncertainty quantification of an MMC is presented. To this end, first sensitivity analysis is conducted to identify the key parameters whose tolerances contribute the most to the parametric uncertainty of the selected design variables. Second, the effect of increasing the number of power cells in each arm on the estimated total uncertainty, and thus the predictive capability of the MMC simulation models for medium- and high-voltage applications is studied. A simplified testbed for model validation of the power cell in the design of an MMC is developed accordingly. The development of this simplified testbed allows validating the models used and estimating uncertainties in the design with less computational cost and hardware prototyping.**

***Index Terms*—Design margin, design under uncertainty, model-form uncertainty (MFU), modeling, modular multilevel converter (MMC), parametric uncertainty (PU), uncertainty quantification.**

I. Introduction

THE modular multilevel converter (MMC) has become a preferred choice for medium- and high-voltage applications as it has several advantages compared with two-, three-, and multilevel voltage source converters [3]–[5]. Advantages, such as a nearly ideal current and voltage scalability, excellent harmonic performance, and distributed energy storage, have made this converter the most promising converter technology developed in recent years. A well-known adaptor of this converter has been high-voltage direct-current (HVdc) transmission systems [6]–[9].

Power cells in an MMC—a full-bridge or half-bridge circuit—can be configured as a power electronics building block or PEBB. The concept of PEBB encompasses the integration of fundamental components including power devices, gate drives, and the minimum required passive components as well as control schemes [10], [11]. PEBB as a concept to construct modular converters was initially proposed by the Office of Naval Research in 1997 [12]. Over the past two decades, PEBB-based modular converters have gained increased attention due to their minimal maintenance cost, easy assembly, and production [13], [14].

The circuit configuration of a three-phase PEBB-based MMC is shown in Fig. 1. Each phase of the converter consists of two arms, the upper and the lower. Each arm comprises a number of series-connected PEBBs. In this article, as shown in Fig. 1, the PEBB is configured as a full-bridge, not the conventional half-bridge, due to its several advantages, namely four-quadrant operation, fault handling capability, and small impact when fewer PEBBs are used in each arm in medium-voltage applications, as opposed to hundreds in the HVdc case.

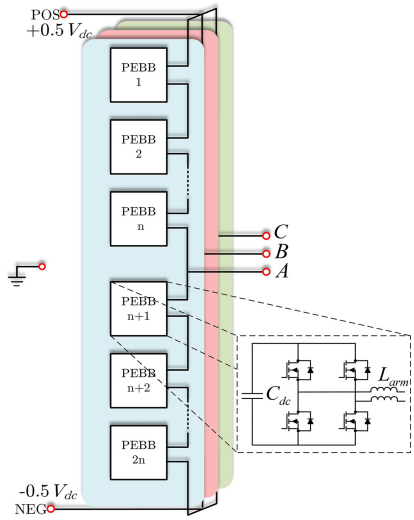

Fig. 1. Circuit configuration of the MMC.

Manuscript received July 27, 2019; revised October 25, 2019 and January 15, 2020; accepted February 24, 2020. Date of publication March 11, 2020; date of current version June 23, 2020. This paper was presented in part at the IEEE Applied Power Electronics Conference and Exposition, Tampa, FL, USA, March 2017 [1], and in part at the IEEE Energy Conversion Congress and Exposition, Cincinnati, OH, USA, October 1–5, 2017 [2]. Recommended for publication by Associate Editor Z. Li. *(Corresponding author: Niloofar Rashidi.)*

Niloofar Rashidi, Rolando Burgos, and Dushan Boroyevich are with the Department of Electrical and Computer Engineering, Virginia Polytechnic Institute and State University, Blacksburg, VA 24061 USA (e-mail: rashidim@vt.edu; rburgos@ieee.org; dushan@vt.edu).

Chris Roy is with the Department of Aerospace and Ocean Engineering, Virginia Polytechnic Institute and State University, Blacksburg, VA 24061 USA (e-mail: cjroy@vt.edu).

Color versions of one or more of the figures in this article are available online at http://ieeexplore.ieee.org.

Digital Object Identifier 10.1109/TPEL.2020.2980000

Component selection, modulation implementation, and control algorithm are a few examples of several aspects of MMCs that require crucial insight and understanding of the converter operation and its dynamics. At early design stages modeling and simulation, as a set of design and development tools, provide valuable perspectives on these aspects. They represent the fastest and safest way to study a circuit or system, aiding in the research, design, diagnosis, and the elimination of unforeseen errors in the development of power converters [15]. Further, in the process, and prior to mass production, the converter design also needs to be verified via model-based reliability and production yield analysis, i.e., worst-case analysis [16] and design for Six Sigma [17]. These analyses ensure that the system performance will meet design specifications even with the expected variations in operating conditions and parameter values. In other words, the above-mentioned computer-aided design tools try to determine the effects of parameter variation on the circuit performance; this effect is known as parametric uncertainty (PU).

Yet, PU is not the only source of variation in the design; the credibility of the design achieved with model-based techniques strongly depends on the accuracy of the simulation models themselves, which is not addressed in any of the aforementioned types of manufacturing-oriented analysis. Instead, heuristic safety factors are often used to compensate for the possible deviation of real system performance from the predictions made using modeling and simulation. This deviation, however, can be effectively quantified by comparing simulation and experimental results in what is known as model-form uncertainty (MFU).

In [18], modeling and design with parametric and model-form uncertainty quantification (P&MF-UQ) were proposed as an alternative design approach. This approach aims at quantifying the main sources of uncertainty in the modeling and design of a power converter for which experimental results for MF-UQ and nondeterministic simulation results for parametric uncertainty quantification (P-UQ) are obtained. This approach is capable of building confidence in modeling and simulation results in the presence of manufacturing variability as well as modeling inaccuracies and could potentially eliminate the need for heuristic safety factors.

Accordingly, the goal of this article is to improve the existing modeling practice and validate the models used in the design of an MMC using modeling and design with P&MF-UQ. The mathematical model of the MMC is presented in Section II, where the description of the component modeling, modulation implementation, and controller scheme is provided. In Section III, the enhanced modeling framework is reviewed where PU and MFU are discussed. Since estimating PU and MFU for large-scale power converters and systems such as MMCs requires a significant computational effort and hardware prototyping, UQ analysis as a key step in the design with P&MF-UQ could potentially impose limitations concerning the feasibility of the approach; these limitations are discussed in Section IV. In Section V, a systematic study is conducted to develop a simplified testbed for UQ analysis and model validation in the design of an MMC. In this section, the effect of adding more PEBBs on the accuracy and thus the predictive capability of MMC simulation models is investigated and a simplified testbed for UQ analysis is developed accordingly. In Section VI, the minimum required margin for the selected design variables at the full-power operating condition is calculated using the developed simplified testbed, which on one hand allows estimating effects of parameters variation with the minimum computational costs, and on the other hand enables estimating modeling inaccuracy by running scaled-down validation experiments. Finally, the conclusion is drawn in Section VII.

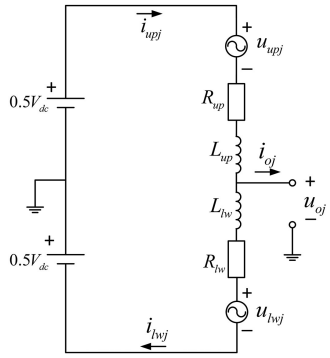

Fig. 2. Equivalent circuit of one phase of the MMC.

II. Modulation Implementation and Control Algorithm

The equivalent circuit of one phase of an MMC, shown in Fig. 2, is used for the analysis provided in this section; the other two phases have a similar behavior. The following equations can be obtained by Kirchhoff's voltage law:

$$\frac{1}{2}V_{\rm dc} = u_{\rm upj} + R_{\rm up}i_{\rm upj} + L_{\rm up}\frac{di_{\rm upj}}{dt} + u_{\rm oj} \tag{1}$$

$$\frac{1}{2}V_{\rm dc} = u_{\rm lwj} + R_{\rm lw}i_{\rm lwj} + L_{\rm lw}\frac{di_{\rm lwj}}{dt} - u_{\rm oj} \tag{2}$$

where $u_{\rm oj}$ is the output voltage of phase *j* (*j* ∈{*a, b, c*}), $i_{\rm oj}$ is the phase current, and $V_{\rm dc}$ is the dc-link voltage. Variables $u_{\rm upj}$, $i_{\rm upj}$, $u_{\rm lwj}$, and $i_{\rm lwj}$ represent the voltages and currents of the upper and lower arms, respectively. $R_{\rm up}$, $R_{\rm lw}$, $L_{\rm up}$, and $L_{\rm lw}$ are the resistances and inductances of the upper and lower arms, respectively. Therefore, the expression for output voltage can be derived as

$$u_{\rm oj} = \frac{1}{2}(u_{\rm lwj} - u_{\rm upj}). \tag{3}$$

Furthermore, $i_{\rm Zj}$ is defined as the circulating current along the *j*-phase and based on the definition, it only circulates in-between phase-legs without flowing to the dc-bus or the ac line. The circulating current along the *j*-phase can be given by

$$i_{\rm circj} = \frac{1}{2}(i_{\rm upj} + i_{\rm lwj}). \tag{4}$$

The arm currents, in turn, can be expressed in terms of the circulating current and the phase current as

$$i_{\rm upj} = i_{\rm circj} + \frac{1}{2}i_{\rm oj} \tag{5}$$

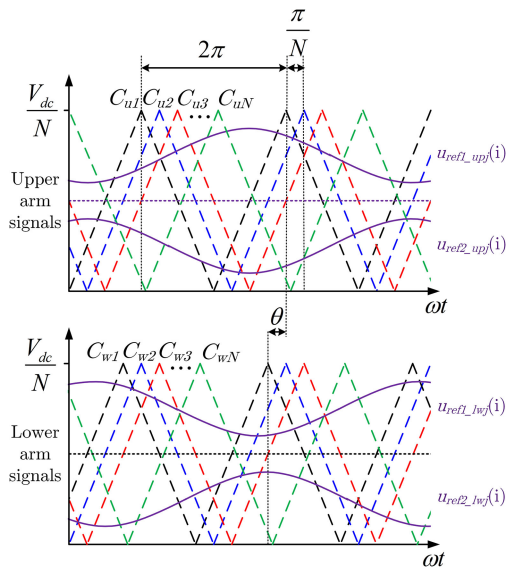

Fig. 3. Interleaved carrier pulse width modulation signals of phase j of an MMC with N PEBBs per arm: $2N$ triangular carrier with the frequency of $f_{\rm sw}$ and $2N$ reference signals with the line frequency are generated in total.

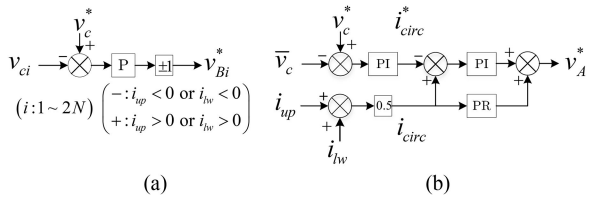

Fig. 4. Block diagram of dc-capacitor voltage control. (a) Balancing controller. (b) Averaging controller.

$$i_{\rm lwj} = i_{\rm circj} - \frac{1}{2} i_{\rm oj}. \tag{6}$$

The phase-shifted carrier modulation technique, shown in Fig. 3, is used in this article, where the N triangular carriers of upper/lower arms (C_{u1}, C_{u2}, ..., C_{uN} for the upper arm, and C_{w1}, C_{w2}, ..., C_{wN} for the lower arm) are shifted by π/N incrementally to achieve the best harmonic cancellation [19]. Each PEBB is assigned with a specific reference signal and a triangular carrier, such that all PEBBs have the same switching frequency, thereby the semiconductor stress is evenly distributed. As the PEBBs of this converter are modulated independently, the voltage balancing of the capacitors can be achieved by adjusting the reference signal of each PEBB. The complete block diagram of the capacitor voltage balancing method is shown in Fig. 4. The controller used in this article is adapted from [21] and is composed of an averaging controller together with a voltage balancing block. As shown in Fig. 4(a), the balancing controller balances individual PEBB voltages with respect to their reference value. The averaging controller [see Fig. 4(b)] forces the j-phase average voltage ($\bar{v}_{\rm cj}$) to follow its command (v_c^*). An ac circulating current control loop (a proportional-resonant controller [22]) with zero current reference, is added to the balancing controller to suppress the second-order harmonics of the circulating current with a minimum effect on the original system performance.

Finally, the switching pulses of each PEBB are generated by comparing the reference signals with the corresponding carrier wave. The reference signals of the upper and lower PEBBs are given by

$$u_{\rm ref1\_}{}_{lwj}(i) = \frac{3V_{\rm dc}}{4} + \frac{MV_{\rm dc}}{4}\cos(\omega_o t + \phi_j) + \Delta u_{\rm ref\_}{}_{lwj}(i) \tag{7}$$

$$u_{\rm ref2\_}{}_{lwj}(i) = \frac{V_{\rm dc}}{4} + \frac{MV_{\rm dc}}{4}\cos(\omega_o t + \phi_j + \pi) - \Delta u_{\rm ref\_}{}_{lwj}(i) \tag{8}$$

$$u_{\rm ref1\_}{}_{upj}(i) = \frac{3V_{\rm dc}}{4} + \frac{MV_{\rm dc}}{4}\cos(\omega_o t + \phi_j + \pi) + \Delta u_{\rm ref\_}{}_{upj}(i) \tag{9}$$

$$u_{\rm ref2\_}{}_{upj}(i) = \frac{V_{\rm dc}}{4} + \frac{MV_{\rm dc}}{4}\cos(\omega_o t + \phi_j) - \Delta u_{\rm ref\_}{}_{upj}(i) \tag{10}$$

where $u_{\rm ref1\_upj(}{}_{lwj)}$ and $u_{\rm ref2\_upj(}{}_{lwj)}$ are the two reference signals for H-bridge of the $i^{\rm th}$ PEBB in the upper(lower) arm, M ($0 < M < 1$) is the modulation index, ω_o is the angular frequency of the output ac voltage, ϕ_j is the phase angle, and $\Delta u_{\rm ref\_upj(}{}_{lwj)}(i)$ is the reference adjustments for the ith PEBB in the upper (lower) arm, which is obtained by the voltage balancing and averaging controller commands (see Fig. 4) as follows:

$$\Delta u_{\rm ref\_}{}_{upj(lwj)}(i) = v_A^*(i) + v_B^*(i). \tag{11}$$

It should be noted that the difference between the phase angle of the triangular carrier in the lower and upper arms (θ), shown in Fig. 3, has a significant impact on the harmonic features of the output voltage and the circulating current [20]. Based on the double Fourier series analysis, the harmonics of the circulating current will be minimized when the displacement angle is π/N and 0 degrees, respectively for the converter with odd and even numbers of series-connected PEBBs per arm.

III. Enhanced Modeling Framework

An enhanced modeling framework for the design of power electronic converters and systems is presented in [18]. This modeling framework ultimately pursues a reduced level of dependence on experimental results, as well as to empower the role of modeling and simulation results in the design and decision-making processes. The proposed modeling framework can quantify the deviation of the real system performance from predictions made using modeling and simulation, a capability that is attained by the proper identification, characterization, and quantification of the different, and often numerous, sources of uncertainty. There are, in fact, two main sources of uncertainty in the modeling and simulation of power converters that are addressed through this framework: PU, which results from manufacturing variability, and MFU, which results from the inherent inaccuracies of the models used. A brief discussion on these main sources of uncertainties is provided below.

A. Parametric Uncertainty

Due to the lack of knowledge about parameters or their inherent variations, the model input parameters, which are the simulation inputs, are usually nondeterministic [23]. As a result, to improve the modeling framework, as the first step, all potential sources of uncertainty in the model input parameters, known as PU, should be quantified. The following describes how this inevitable source of uncertainty is quantified through the modeling framework.

P-UQ is summarized in three main steps: uncertainty identification, characterization, and quantification [24]. After identifying all uncertain model input parameters, a mathematical structure is assigned to each parameter; the uncertain parameter is characterized by either a distribution or an interval depending on its type of uncertainty. In the case of an epistemic uncertainty (due to lack of knowledge), the parameter is characterized by an interval with determined upper and lower limits. If it is aleatory (due to randomness), the parameter is characterized by a probability distribution with its associated parameters. The numerical values of all parameters in the resultant mathematical structures are then determined. A nondeterministic simulation is finally carried out using Monte Carlo (MC) sampling techniques, where samples are taken from a range of the model input parameters, and numerous simulations are run to generate a sequence of system response quantities (SRQs). Finally, to present the PU with an interval in the final prediction of the SRQ, an arbitrary interval-valued probability, e.g., a capability index of two-sigma (95% level of confidence), needs to be selected.

One important concept in the nondeterministic simulation is what is known as the curse of dimensionality, which refers to the increase in the number of samples needed as the number of uncertain parameters increases [25]. This would in effect result in an increase in the number of the model evaluation required in performing MC simulations. Considering an MMC with a large number of series-connected PEBBs, performing MC simulations would be extremely expensive or nearly impossible in terms of computational costs due to the huge number of uncertain model input parameters.

Sensitivity analysis (SA) reduces the input parameters to those that significantly affect the SRQ, so those that do not have a major effect can be neglected. In this article, among different techniques, analysis of variance (ANOVA) is used to examine the effectiveness of different parameters on the selected SRQs. Sobol indices are then calculated based on ANOVA formulation providing both the first-order and total effect metrics [26]. The total effect metric measures the contribution to the output variance from an input including a first-order effect plus any higher order effects caused by interaction with other inputs. The total effect is thus the primary metric of interest in the SA as it indicates fixing what input at its nominal value will provide the greatest reduction in output variance. Therefore, in MC simulations, parameters with the first-order and total effects of close to zero can be kept constant at their nominal values.

In the following, the model under investigation is described by a function that is $y = f(\mathbf{x})$, where the input $\mathbf{x}$ ($\mathbf{x} = [x_1, x_2, \ldots, x_n]$) is a point inside an *n*-dimensional input space, and y is a scalar output. The first-order and total effect indices are calculated using equations below

$$S_i = \frac{V_{x_i}\left[E_{\mathbf{x}_{\sim i}}\left(y|x_i\right)\right]}{V(y)} \tag{12}$$

$$S_{Ti} = \frac{E_{\mathbf{x}_{\sim i}}\left[V_{x_i}\left(y|\mathbf{x}_{\sim i}\right)\right]}{V(y)} \tag{13}$$

where the meaning of the inner operator ($E_{\mathbf{x}_{\sim i}}(.)/V_{x_i}(.)$) is that the mean/variance of y is taken over all possible values of $\mathbf{x}_{\sim i}/x_i$ while keeping $x_i/\mathbf{x}_{\sim i}$ fixed; the outer operator ($V_{x_i}(.)/E_{\mathbf{x}_{\sim i}}(.)$) is then the variance/mean taken over all possible values of $x_i/\mathbf{x}_{\sim i}$.

To compute sensitivity indices using the above formulae, however, the number of model evaluations strictly depends upon the number of uncertain parameters. Besides, according to (12) and (13), two computation loops are required to calculate first- and total-effect indices. In the case of an orthogonal input space, however, the computations could be much more accelerated. In [27] alternative formulas are derived to compute S_i and S_{Ti} simultaneously for an orthogonal input space without requiring a separate set of model evaluations for each index. These formulas, known as Jansen estimators, are MC-based estimators and are given as

$$S_i = \frac{V(y) - \frac{1}{2M}\sum_{j=1}^{M} f(B)_j f(A_B^{(i)})_j}{V(y)} \tag{14}$$

$$S_{Ti} = \frac{\frac{1}{2M}\sum_{j=1}^{M}(f(A)_j - f(A_B^{(i)})_j)^2}{V(y)} \tag{15}$$

where, A and B are two $K \times M$ sampling matrices generated from a quasi-random sequence of size $M \times 2K$; K is the number of uncertain parameters and M is the number of samples taken from each parameter. In matrix $A_B^{(i)}$ ($B_A^{(i)}$) all the columns are from $A(B)$ except for the i^{th} column which is from $B(A)$.

B. Model-Form Uncertainty

As discussed earlier in this article, the validity of modeling and simulation results fully relies on the accuracy of the models used. This source of uncertainty is often neglected or estimated by heuristic safety factors in the final simulation results. Hence, to further empower the role of modeling and simulation in decision-making, the uncertainty due to modeling inaccuracy, known as MFU, is also included in the proposed modeling approach [18].

The validation metric is a methodology used to measure the MFU. Preferably, MFU should be measured based on experimental results from distribution of hardware prototypes and their corresponding simulation result, which is obtained from MC simulation. When only aleatory uncertainties are present in the model inputs, then propagating these uncertainties through the model produces a simulated cumulative distribution function (CDF) of the SRQ. Experimental measurements are then used to construct an empirical CDF of the SRQ. The modified area validation metric (MAVM), that is the validation metric used in this article, separately tracks the regions between two CDFs (see Fig. 5) [28]. Specifically, the region where the experimental values are larger than the simulation values is referred to as "d^+," and the region where the experimental values are smaller than

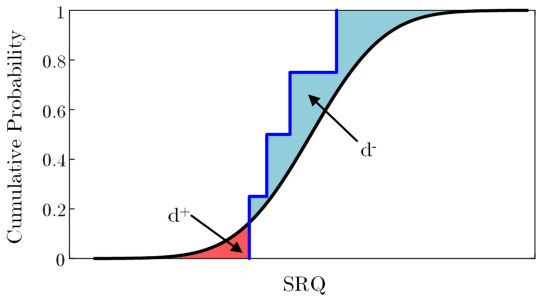

Fig. 5. MAVM example.

the simulation values is referred to as "d^-." The estimated MFU is the summation of the absolute values of d^+ and d^-, and has the same unit as the selected SRQ. In addition to MFU, the MAVM also provides an estimate of model-form error (MF error), ϵ_{MF}, which is the difference between d^- and d^+.

IV. Design With Uncertainty Quantification

The modeling framework described in the previous section quantifies the deviation of the real system performance from predictions made using modeling and simulation, a capability that is attained by quantifying PU and MFU. In fact, a design methodology based on this enhanced modeling framework, that is designed with P&MF-UQ, represents a desirable alternative to the design of MMCs. This approach aims at quantifying all sources of uncertainty in an MMC for which experimental results for MF-UQ and nondeterministic simulation results for P-UQ are required.

As such, unlike other model-based design techniques, this approach considers modeling inaccuracies as well as the parameter tolerances in determining the required design margin. In early design stages, a limited number of hardware prototypes are built and tested using the design of the experiment to ensure the mass-produced version meets qualification testing standards. The ultimate goal of P&MF-UQ is to use these experimental results and the nondeterministic simulation results at early design stages to estimate the total uncertainty in the modeling and design of the converter. This type of design approach would expectedly yield less conservative and more dependable designs without requiring any additional resources. Yet, the utilization of this technique will effectively eliminate the need for heuristic safety factors, yielding quantifiably more precise designs that are capable of truly maximizing the power processing capability.

However, UQ analysis, as a key step in the design with P&MF-UQ, could potentially apply limitations concerning feasibility; these limitations are briefly discussed in the following.

There are two main factors affecting the computational cost of a nondeterministic simulation: the number of model evaluations required, and the fidelity of the model. The first factor is a function of the number of uncertain model input parameters where SA results are used to minimize the number of uncertain parameters and accordingly the number of required model evaluations. The latter, however, depends on the level of accuracy required in the context where the model is used. As an example, in the switching model of an MMC for medium-voltage drives or HVdc applications [29], [30], there are tens to thousands of PEBBs connected in series; as more PEBBs are added in each arm, the computational cost per model evaluation increases significantly due to the huge number of PEBBs that are modeled, thereby increasing the overall computation cost per model evaluation. This increase is in addition to the increase in the number of required model evaluations, leading to another challenge in P-UQ.

On the other hand, and with regards to MF-UQ, when it comes to large-scale power converters and systems, testing the complete converter at its rated power could be prohibitively expensive, or sometimes impossible at the early design stage due to safety considerations or physical constraints (equipment, facilities, etc.). Experiments are often carried out using scaled-down laboratory prototypes to complete the modeling effort. For instance, to measure the accuracy of the MMC model, MF-UQ requires conducting a full-power validation experiment on the hardware prototype of the MMC with the actual number of PEBBs. Whereas, a hardware prototype with only a limited number of power modules is usually available at early design stages to run low-power validation experiments [29]. As a result, MF-UQ at the full-rated power lacks experimental results.

Therefore, for UQ analysis of large-scale power converters and systems such as MMCs, a simplified testbed is required. In Section V, first, a study for developing a simplified testbed for conducting both P-UQ and MF-UQ is conducted and a simplified testbed for model validation of the PEBB in the design of an MMC is derived. This simplified testbed enables validating certain aspects of the design with less computational cost and hardware prototyping. Second, the minimum required margin for the selected design variables is calculated based on multiple low-power validation experiments using a regression-based UQ analysis.

V. Simplified Testbed for Model Validation

The goal set forth was to improve the existing modeling practice used in the design of an MMC by means of P&MF-UQ. Due to several challenges of validating an MMC model that could be used in the design of this converter, this section investigates the possibility of validating a PEBB model instead. This would be done so that the corresponding model, with the gained confidence in its simulation results, could be used in the design of the full-fledged MMC.

To develop a simplified testbed for the model validation process in the design of an MMC, the relationship between total uncertainty associated with the SRQs of interest, and the number of PEBBs per arm, needs to be investigated. To this end, the effects of adding more PEBBs per arm on the PU and MFU associated with SRQs are studied separately. It should be noted that the models used in this article are verified using the verification approach discussed in [18].

In this article, high switching frequency high power SiC-based PEBBs are used which has shown to be a promising replacement of conventional Si IGBT-based PEBBs for implementing MMCs in medium voltage applications [14], [31]. This is mainly due to the recent advancements in the development of SiC MOSFET with low switching losses and high switching speed that enable

TABLE I
PEBB SPECIFICATIONS

Parameter	Nominal Value
DC-bus rated voltage	1000 V
DC-bus voltage ripple	150 V
Terminal rms current	5.7 A
Maximum switching Frequency	100 kHz

TABLE II
UNCERTAIN MODEL INPUT PARAMETERS AND THEIR SPECIFICATION

Parameter	Nominal Value	Tolerance (%)
DC capacitance	210 μF	20
DC capacitor ESR	1.2 $m\Omega$	15
Arm inductance	1 mH	25
Arm inductor ESR	25 $m\Omega$	20
AC inductance	1.5 mH	25
AC inductor ESR	40 $m\Omega$	20

high switching frequency operation, which improves the overall power density of the PEBB [13]. This would, however, raise concerns regarding safe the operation of the device. To this end, both the peak dc-bus voltage and the peak arm current of the PEBB are selected as SRQs given that they are two of the main design variables in determining the voltage and current stress of the SiC devices in question. Tables I and II summarize the specifications and circuit parameters of the PEBB under study.

A. Parametric Uncertainty

In this section, the PU of the selected SRQs of MMC is estimated for three cases where the number of PEBBs per arm increases incrementally. The modulation implementation and control system are those presented in Section II. All the model input parameters that are subject to variability are identified as the uncertain input parameters. These uncertainties are mainly due to manufacturing tolerance and natural material variability. A mathematical structure is then assigned to each of these uncertain parameters based on the type of uncertainty. In this case, the uncertain parameters are characterized by a normal distribution with a specific mean and standard deviation which is equal to the nominal value and one-third of the tolerance of each uncertain input parameter, respectively. Table II summarizes the circuit parameters for the Monte-Carlo simulations.

Prior to P-UQ, as mentioned in Section III, the SA is first performed to determine the parameter prioritization based on their contribution to the final SRQ (model output). In complicated systems, such as the MMC, which can be presented in a hierarchical structure, the SA could also be carried out at different levels, including sub-module (PEBB) and system level. Since the operating principles in all three phases are identical and independent from each other, analyses are performed on one phase, and similar results are expected from the two other phases. Table III summarizes the sensitivity indices of the peak dc-bus voltage and peak arm current of a PEBB in an MMC with two PEBBs per arm derived using (14) and (15), where y is the SRQ of interest and $\mathbf{x}$ is the vector of uncertain parameters listed in Table II; similar results are expected for other PEBBs in the phase-leg.

TABLE III
SUMMARY OF SA RESULTS FOR PEAK DC-BUS VOLTAGE AND PEAK ARM CURRENT OF PEBB1 IN THE MMC WITH TWO PEBBs/ARM

Parameter	Peak dc-bus voltage of PEBB 1		Peak arm current of PEBB1 (upper arm)	
	S_i	S_{Ti}	S_i	S_{Ti}
	PEBB level			
Arm inductance, L_{arm}	0	0	0	0.16
Arm parasitic resistance, R_{arm}	0	0	0	0.10
dc-link capacitance, C_{dc}	0.99	0.99	0.83	0.99
dc-link parasitic resistance, R_{dc}	0	0	0	0.10
MOSFET on resistance, R_{ds}	0	0	0	0.12
Diode forward voltage, V_f	0	0	0	0
Diode on resistance, R_d	0	0	0	0
	System level			
PEBB1 Arm inductance, L_{arm1}	0	0	0	0.05
PEBB1 dc-link capacitance, C_{dc1}	0.99	0.99	0.11	0.32
PEBB2 Arm inductance, L_{arm2}	0	0	0	0.05
PEBB2 dc-link capacitance, C_{dc2}	0	0	0.11	0.32
PEBB3 Arm inductance, L_{arm3}	0	0	0	0.05
PEBB3 dc-link capacitance, C_{dc3}	0	0	0.16	0.35
PEBB4 Arm inductance, L_{arm4}	0	0	0	0.05
PEBB4 dc-link capacitance, C_{dc4}	0	0	0.16	0.35
AC inductance, L_{ac}	0	0	0.05	0.15

According to SA results, the uncertain input parameters are reduced to those whose tolerances contribute the most to the PU of the SRQs of interest, namely dc capacitors and arm inductors in each PEBB, and those that do not have a big effect are fixed at their nominal values. In addition, as three phases of the MMC are independent of one another, the PU of the peak dc-bus voltage and the peak arm current of each PEBB can be estimated by propagating only the model input uncertainties of the PEBBs in the same phase. The parameters of the other two phases can be fixed at their nominal values, resulting in a significant reduction of the number of uncertain parameters.

As all input uncertainties are classified as aleatory, the method Latin Hypercube sampling (LHS) is used to sample from the distributions of the model input parameters to generate a sequence of SRQs [32]. Fig. 6 shows the resultant CDF of the peak dc-bus voltage and the peak arm current of one of the PEBBs in one MMC phase-leg. It should be noted that due to the current ripple reduction as a result of having more PEBBs in each arm, the nominal peak arm current decreases as more PEBBs are connected in series. The resultant CDF of the peak arm current for all cases is therefore normalized with respect to its mean value for each case. As shown in Fig. 6(a), the peak dc-bus voltage of any PEBB is independent of the number of

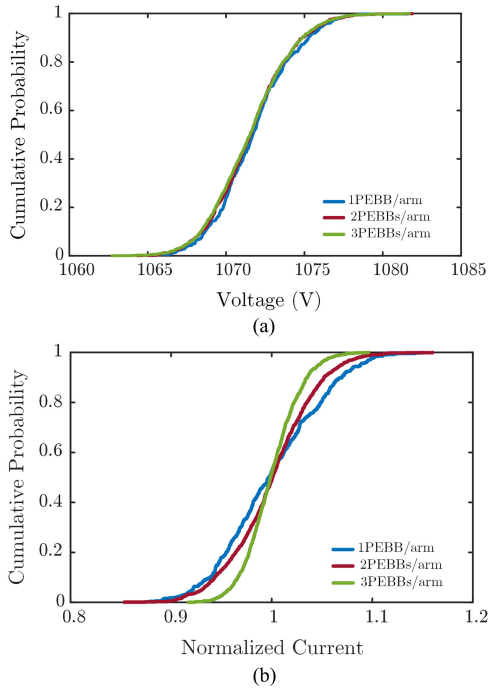

Fig. 6. CDFs of the (a) peak dc-bus voltage, and (b) peak arm current of the PEBB in MMCs with 1, 2, and 3 PEBBs per arm.

TABLE IV
PHASE-LEG SPECIFICATION OF THE SCALED-DOWN VALIDATION EXPERIMENTS

Parameter	PU	
	Case 1	Case 2
Number of PEBB(s) per arm	1	2
Load apparent power [VA]	1000	2000
DC link voltage [V]	180	360
Line frequency [Hz]	60	60
AC line current [A]	10	10

series-connected PEBBs in each arm. When there is peak arm current, however, as shown in Fig. 6(b), the distribution will be affected as more PEBBs are connected in series.

A two-sigma capability index is finally used to demonstrate the PU in the peak dc-bus voltage of the PEBB and the peak arm current. Table IV summarizes the corresponding PU for each of the cases with a 95% level of confidence. This result unveils an interesting feature of the MMC; the PU of the peak arm current will decrease as more PEBBs are added in series to scale up the voltage for different applications. The PU of the peak dc-bus voltage of each PEBB, on the other hand, remains the same.

B. Model-Form Uncertainty

As the three phase-legs in an MMC are independent from each other, the needed validation experiments can be conducted on a half-bridge type MMC (single-phase converter). Due to the limited number of PEBBs available, scaled-down validation experiments are conducted for two cases: a phase-leg with one PEBB per arm, and a phase-leg with two PEBBs per arm. Fig. 7

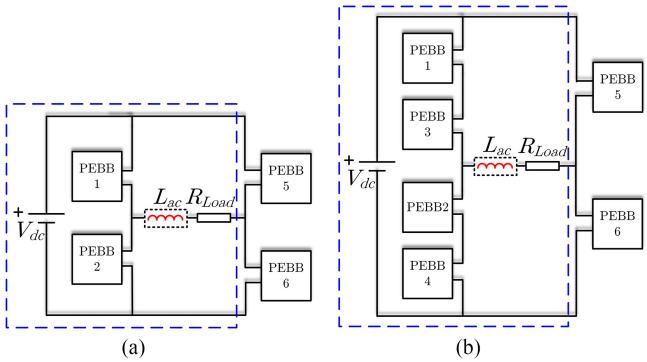

Fig. 7. Experimental circuit for: (a) Case 1: 1 PEBB/arm and (b) Case 2: 2 PEBBs/arm.

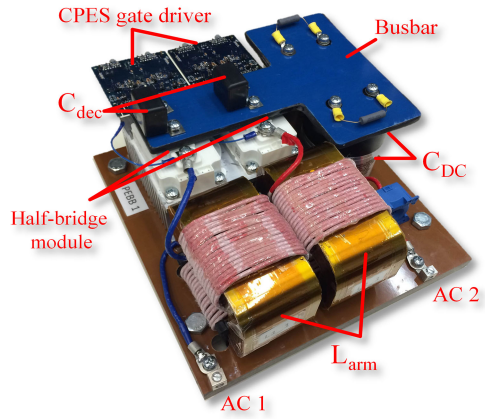

Fig. 8. PEBB hardware prototype.

shows the system configuration used for validation experiments. In the validation experiment setup, for both cases, a second phase-leg (PEBB 5 and PEBB 6 in Fig. 7) is used for the midpoint connection.

Fig. 8 depicts one of the six PEBB units built [33], where the PEBB planar dc-bus structure, film capacitor bank, gate-driver units with high-EMI immunity, and dual-purpose differential- and common-mode inductors are observed. Each PEBB has a power rating of 7.5 kW and a dc-bus voltage rating of 1 kV, operating at a switching frequency of 100 kHz using 1.7 kV SiC MOSFET power modules.

The modulation implementation and control system are the same as those presented in Section II. Tables II and IV summarize the PEBB and phase-leg specifications for the scaled-down validation experiments. These were carried out under the condition of 180 V–1 kW and 360 V–2 kW for the one and two PEBBs per arm cases, respectively. Fig. 9(a) and (b) shows the experimental waveforms of the converter indicating peak dc-bus voltage and peak arm current that are the SRQs of interest. In this article, replicated experimental measurements are provided to consider the uncertainty due to measurement errors. Fig. 10(a) and (b) shows the CDF generated from these measured SRQs.

As described, the experimental measurements are limited to a single hardware unit for each of the cases shown in Fig. 7. Therefore, the empirical CDF in Fig. 10 is not representing the

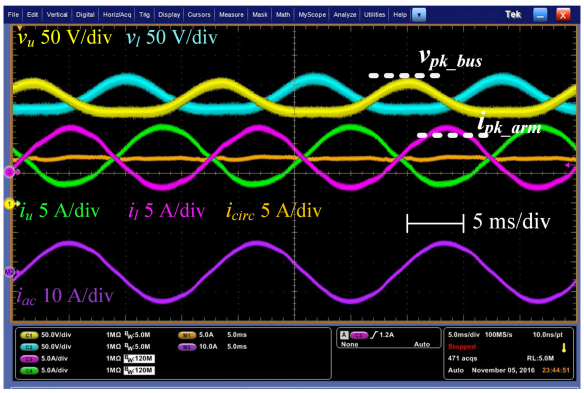

(a)

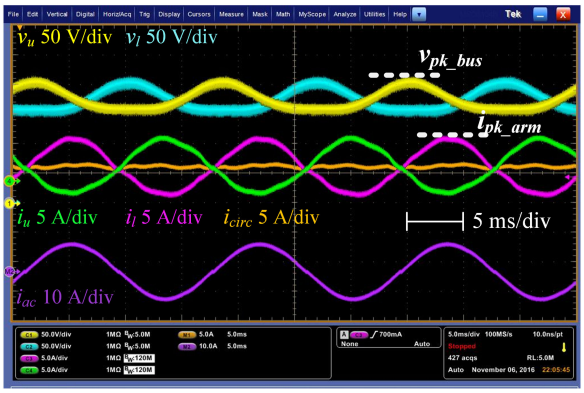

(b)

Fig. 9. Multiple experimental waveforms of the phase-leg with (a) 1 PEBB per arm and (b) 2 PEBBs per arm: A PEBB dc-bus voltage of upper arm v_u, an upper arm current i_u, a PEBB dc-bus voltage of lower arm v_l, a lower arm current i_l, an ac (load) current $i_{\rm ac}$, and a circulating current $i_{\rm circ}$. SRQs of interest: A peak dc-bus voltage v_{pk_bus} and a peak arm current i_{pk_arm}.

TABLE V
CALCULATED PARAMETRIC AND MODEL-FORM UNCERTAINTIES (ABSOLUTE VALUE AND PERCENTAGE) FOR TWO CASE-STUDIES WITH 1 AND 2 PEBBs/ARM (*N* IS THE NUMBERS OF PEBBs PER ARM)

Uncertainty type	PU		MFU	
N / SRQ	1	2	1	2
Peak dc-bus voltage, v_{up1}	8.4 V (3.8%)	8.4 V (3.8%)	9.39 V (4.3%)	9.40 V (4.3%)
Peak arm current, i_{up}	1.6 A (18.3%)	1.3 A (15%)	1.25 A (14.3%)	1.00 A (11.5%)

CDF from simulation results shown in Fig. 6. A proper replication of the CDF, shown in Fig. 6, requires multiple experimental units available. Therefore, a single simulation using the measured value of all parameters of the PEBBs is used to calculate the MFU. Fig. 10 shows the CDFs from simulation and experiment representing the peak dc-bus voltage of the PEBB (PEBB 1), and the peak arm current (upper arm) for both cases: one PEBB per arm and two PEBBs per arm. The enclosed region between each pair of CDFs from simulation and experiment is then estimated where d^+ and d^- are calculated separately.

Table V summarizes the estimated MFU associated with the predictive capability of the model in predicting the PEBB peak dc-bus voltage and peak arm current as evidenced by the validation assessment on the available data for both cases. The MFU of the peak dc-bus voltage of the PEBB is the same for both cases. However, the MFU of the peak arm current decreases when the number of PEBBs in each arm is increased to two.

C. Total Uncertainty and Discussion

The sum of the estimated MFU and PU in the previous sections, based on the two-sigma capability index, is the total uncertainty in modeling and simulation of the MMC with a 95% level of confidence. The total uncertainty is the expected amount of variation in the system performance from predictions made from modeling and simulation results.

As shown in Table V, the total uncertainty associated with the final prediction of the peak dc-bus voltage is independent of the number of series-connected PEBB in each arm of the MMC. Therefore, the estimated range for a phase-leg with one PEBB per arm could be used as the estimated uncertainty for the case of a three-phase MMC with more PEBBs per arm.

However, when there is peak arm current, the PU and MFU will be affected as more PEBBs are connected in series. A regression-based model could be developed to predict the PU of the MMC with more PEBBs per arm. Besides, the estimated PU of the peak arm current of a single phase-leg with one PEBB per arm can be used as the upper bound for the final prediction of this SRQ in other cases that have more series-connected PEBBs.

Although the estimated MFU is limited to 2PEBBs/arm, the trends observed in total uncertainty are corroborated through additional simulation studies and SA as indicated earlier in this section.

Based on the analysis given in this section, in the design of MMC, having more PEBBs in each arm does not necessarily require a greater margin for the selected design variables of interest. A single phase-leg with one PEBB per arm can be used in the case of the SRQs in question as a simplified testbed for model validation in the design of an MMC without introducing any further uncertainties into the modeling and simulation. Accordingly, the heuristic safety factors in the design of MMC can be replaced by the estimated total uncertainty at the full-rated power for the selected design variables using the simplified testbed. This may result in further minimizing the design margins and improvements, while the safe operation of the converter is ensured via the gained confidence in the predictive proficiency of MMC simulation models.

VI. REGRESSION-BASED DESIGN MARGIN ESTIMATION

In a design with P&MF-UQ, the minimum required design margin is determined based on the estimated total uncertainty at the full-rated power of a power converter or system. Consider a case where testing the PEBBs developed for the simplified testbed at their full-rated power is not possible. PU can still be estimated using MC simulation at the full-power condition using a simplified testbed. Whereas, estimating the MFU is limited to a narrow operating range; and the comparison between simulation and experimental results at full-rated power lacks the required experimental results. In this case, since the application domain is outside of the validation domain, an extrapolation procedure

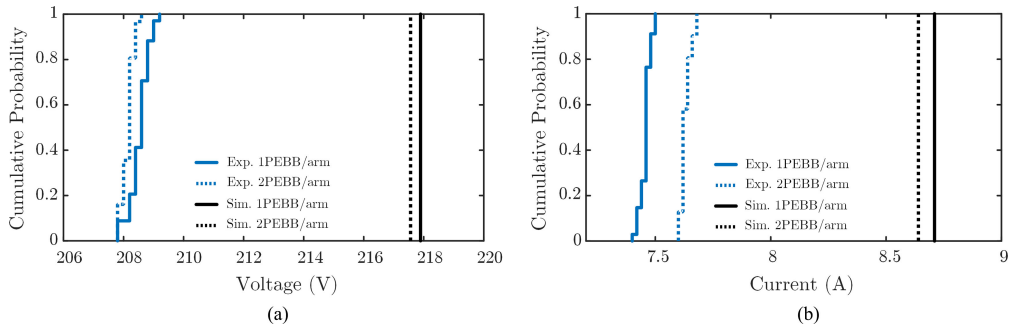

Fig. 10. CDFs of the PEBB (a) peak dc-bus voltage and (b) peak arm current from simulation and experiment. The enclosed area between dashed line is the modeling error of the switching model of the MMC with 1 PEBB/arm and the enclosed area between solid lines shows the modeling error of the MMC with 2 PEBBs/arm.

must be used using a regression model for MFU estimation in the application domain [34]. As a result, MFU is based directly on what has been observed in the prediction performance of the model at low-power validation experiments.

A. Design of Experiments

An essential step in developing a regression model is data collection where a design of experiments (DOE) can be used. DOE is a systematic approach for collecting data used in statistical analysis. The validity of the predictions made outside of the validation domain depends on the quality of the conducted DOE; some of the designs are full factorial, fractional factorial, central composite, one factor, etc. [35].

In this article, full factorial DOE with two factors is applied to evaluate the interaction effect among factors as well as their individual main effect on the accuracy of the model. The first factor is the input dc voltage and the second one is the load rms current. These two are the primary means of changing the power level of validation experiments. Each factor has four levels, where $v_{\text{in,dc}} = \{150, 200, 250, 300\}$ [V] and $i_{L,\text{rms}} = \{3.4, 4.2, 5.7, 8.4\}$ [A]; thus, the total number of sixteen treatment combinations are studied in this section.

The hardware prototype described in Section III is configured as an MMC with one PEBB per arm. Validation experiments are conducted on the simplified testbed at a total number of sixteen different operating points.

B. Model-Form Uncertainty Quantification

In the following, the modeling accuracy needs to be evaluated at sixteen different operating points. Following the same approach discussed in Section III, at each operating condition, d^+ and d^- of the peak dc-bus voltage and peak arm current of PEBB, respectively, are calculated using the 24 measured data and the simulation results, as shown in Fig. 11.

C. Model-Form Error Prediction

The calculated MFU needs to be extrapolated to the full-power condition using a predictive model. The predicted MFU is hence based directly on what has been observed in the prediction performance of the model during low-power validation experiments. In this specific example, and due to the lack of hardware

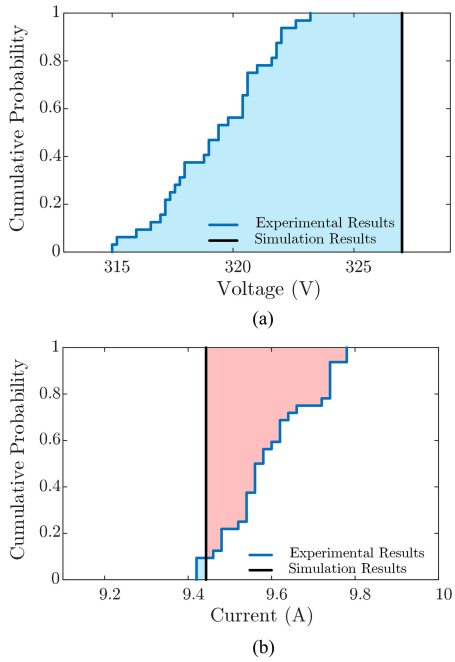

Fig. 11. CDFs of PEBB 1 (a) peak dc-bus voltage and (b) peak arm current from simulation and experiment at 300 V dc-bus voltage and 8.4 A rms load current indicating MFU (d^-, blue-shaded region, and d^+, red-shaded region).

replicates, MF error is used for evaluating modeling accuracy. Therefore, extrapolated MF error at full-power condition will be later used to generate the final P-box. In the case of multiple hardware units, however, d^+ and d^- should be extrapolated separately and used to generate the final P-box.

In this article, Gaussian process regression is used to develop a regression-based predictive model. This method is a simple nonparametric nonlinear regression tool that is widely used in various application areas; it is an alternative for parametric regression tools [36]. This method gives a prior probability to every possible function, where higher probabilities are given to functions that are considered to be more likely. This prior distribution is then conditioned on the training dataset, and a posterior distribution is finally derived over all possible functions. A complete discussion on GP regression tools is provided in [37]. Following the same procedure, a GP regression is developed for the peak dc-bus voltage and peak arm current using the sixteen training data points, which yields sixteen estimated MF errors.

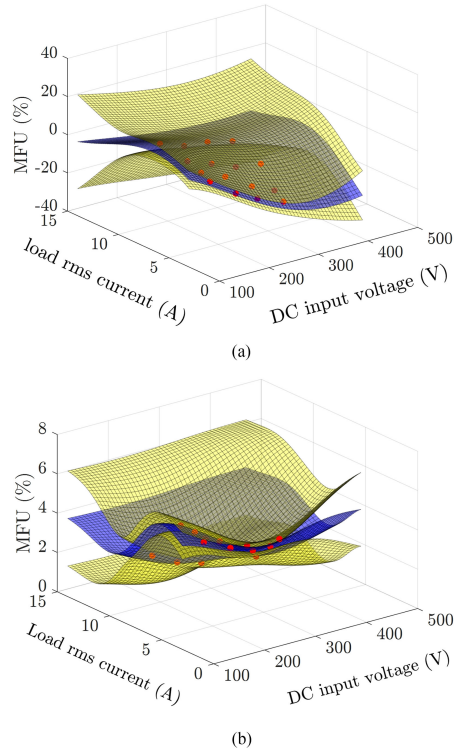

Fig. 12. Mean of the estimated MF error (blue plane) using GP and its 95% PI (yellow planes) as a function of load rms current and dc input voltage for (a) peak dc-bus voltage and (b) peak arm current; red points indicate the training data points.

Equation (16) denotes the GP regression model specified by its mean and covariance functions that are $m(\mathbf{x})$ and $k(\mathbf{x}, \mathbf{x}')$, respectively

$$\mathrm{MFU}(\mathbf{x}) \sim \mathrm{GP}(m(\mathbf{x}), k(\mathbf{x}, \mathbf{x}')) \tag{16}$$

where $\mathbf{x}$ is the vector of operating conditions at which the MFU needs to be estimated, and $\mathbf{x}'$ is the vector of training dataset that is the operating conditions at which the MFU data is available. The covariance function specifies the covariance between pairs of outputs as a function of the inputs. Among possible options for the covariance function, a squared exponential covariance function is selected due to the smooth function behavior that is expected for the MF error over different operating conditions. The associated hyper parameters with the covariance function are then calculated using maximum likelihood [36]. The mean function is first assumed to be zero; however, this can be later modified if needed, so it is not a drastic limitation as the mean of the posterior process is not confined to zero.

Furthermore, in this case, the training dataset is considered to be noisy due to inevitable measurement errors. As a result, the error bound would not be zero at the training data points but has a minimum value. Moving away from the training data points, the error bound increases. More training data points are thus required to reduce the error bound associated with the estimated MF errors. GP finally defines a posterior distribution over all possible functions conditioned on the training dataset. A 95% prediction interval (PI) is selected to calculate an error bound for the predicted MFUs. Fig. 12 shows the mean response of the estimated MFU associated with the peak dc-bus voltage and peak arm current against the dc input voltage and load rms current using the developed GP model, where the 95% PI for the value of the area metric at the regulatory conditions is also shown.

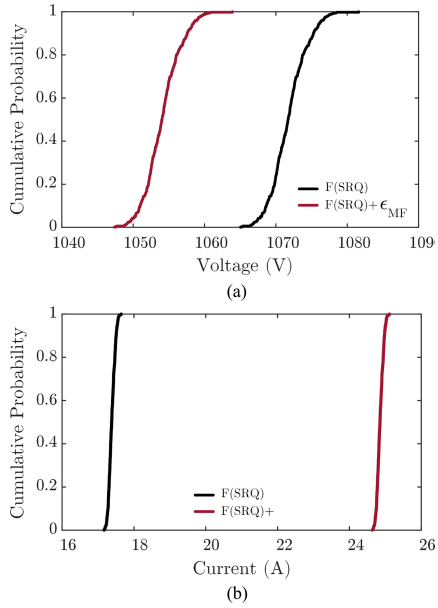

Fig. 13. P-box of PEBB1 (a) peak dc-bus voltage and (b) peak arm current.

The experimental result at a power level beyond the training dataset, namely 450 V dc-bus voltage and 10 A rms load current, is also obtained to evaluate the predictive capability of the GP regression model. At this specific power, the measured MF error is 4.21% and 1.21% for peak dc-bus voltage and peak arm current, respectively. The predicted range for MF error of peak dc-bus voltage and peak arm current using GP is estimated to be 1.77%–6.57% and −31.23%–15.02% that encompass the MF errors from actual measurements and thus verifies the predictive capability of the regression model. Finally, using the GP regression model, the MF error at the full-rated power, i.e., 1000 V dc-bus voltage and 12.8 A rms load current, would be 1.65%–6.49% and –42.97%–30.05% for peak dc-bus voltage and peak arm current, respectively.

D. Final Design Margin

To estimate the final design margin, the upper bound from the PIs at the rated power using GP is used as the estimated MF error. Fig. 13 shows the prediction distribution, representing the input uncertainty, with a parallel distribution displaced by the predicted MF error at the full-power condition. The p-box represents a reasonable estimate of the combined PU and MFU associated with the predictive capability of the model as evidenced by the validation assessment on the available data at low-power condition. The interval-valued probability of 95% is finally used to demonstrate the total uncertainty in the peak dc-bus voltage and peak arm current. Specifically, the model in question predicts the peak dc-bus voltage and peak arm current to be within 1050–1077 V and 17.2–25.1 A, respectively, by taking into consideration the uncertainties of system parameters,

model form, and measurements, at two sigma capability index, evincing the inherent potential of using this predicted range as a design margin without requiring heuristic safety factors.

VII. Conclusion

In this article, modeling and design with P&MF-UQ were used to improve the existing modeling practice and to validate the model used in the design of an MMC. To this end, the main limitations in applying UQ-based design techniques to such large-scale power converters and systems were first discussed. The effect of increasing the number of PEBBs in each arm on the estimated total uncertainty, the predictive capability of the MMC simulation models, and thus the trustworthiness of the design concerning two main design variables, the peak dc-bus voltage and peak arm current of the PEBB, was then investigated. The result revealed an interesting feature of MMCs: although the potential sources of uncertainty increase by adding more PEBBs in each arm, the total uncertainty associated with the final prediction of the selected design parameters remains the same or decreases, depending on the model output. Accordingly, a simplified testbed for UQ analysis and model validation of the PEBB in the design of an MMC was developed. This simplified testbed enabled validating certain aspects of the MMC design with less computational cost and hardware prototyping. Specifically, it was used to conduct MC simulation to estimate PU, and it was also used to conduct scaled-down validation experiments to quantify the MFU at multiple low power conditions. These results were used to build a Gaussian Process regression model and ultimately predict the minimum required design margin at the rated power, with which it was shown how the converter behavior can be predicted with a predefined level of confidence and its design further improved.

References

[1] N. R. Mehrabadi, R. Burgos, C. Roy, J. Yu, and D. Boroyevich, "Study of the predictive capability of modular multilevel converter simulation models under parametric and model form uncertainty," in *Proc. IEEE Appl. Power Electron. Conf. Expo.*, 2017, pp. 1062–1069.

[2] N. R. Mehrabadi, R. Burgos, D. Boroyevich, and C. Roy, "Modeling and design of the modular multilevel converter with parametric and model-form uncertainty quantification," in *Proc. IEEE Energy Convers. Congr. Expo.*, 2017, pp. 1513–1520.

[3] B. Li, S. Zhou, D. Xu, S. Finney, and B. Williams, "A hybrid modular multilevel converter for medium-voltage variable-speed motor drives," *IEEE Trans. Power Electron.*, vol. 32, no. 6, pp. 4619–4630, Jun. 2017.

[4] B. Li *et al.*, "An improved circulating current injection method for modular multilevel converters in variable-speed drives," *IEEE Trans. Ind. Electron.*, vol. 63, no. 11, pp. 7215–7225, Nov. 2016.

[5] S. Du, B. Wu, N. Zargari, and Z. Cheng, "A flying-capacitor modular multilevel converter (fc-mmc) for medium-voltage motor drive," *IEEE Trans. Power Electron.*, vol. 32, no. 3, pp. 2081–2089, Mar. 2017.

[6] T. J. Hammons *et al.*, "Role of HVDC transmission in future energy development," *IEEE Power Eng. Rev.*, vol. 20, no. 2, pp. 10–25, Feb. 2000.

[7] L. Willis and N. Stig, "HVDC transmission: Yesterday and today," *IEEE Power Energy Mag*., vol. 5, no. 2, pp. 22–31, Mar./Apr. 2007.

[8] "HVDC PLUS: The smart way—One step ahead," in *Proc. IEEE ISIE*, 2010, pp. 1–29.

[9] B. Jacobson, P. Karlsson, G. Asplund, L. Harnefors, and T. Jonsson, "VSC-HVDC transmission with cascaded two-level converters," in *Proc. CIGRÉ Session*, 2010, pp. 1–8.

[10] T. S. Ericsen, "Physics based design, the future of modeling and simulation," *Acta Polytechnica*, vol. 45, no. 4, pp. 59–64, 2005.

[11] T. Ericsen, Y. Khersonsky, P. Schugart, and P. Steimer, "PEBB- Power electronics building blocks, from concept to reality," in *Proc. 3rd IET Int. Conf. Power Electron., Mach. Drives*, 2006, pp. 12–16.

[12] T. Ericsen, "Power electronics building blocks," in *Proc. IME/IEE/SEE Electric Warship Conf.*, 1997.

[13] I. Cvetkovic *et al.*, "Modular scalable medium-voltage impedance measurement unit using 10 kV SiC MOSFET PEBBs," in *Proc. IEEE Electric Ship Technol. Symp.*, 2015, pp. 326–331.

[14] J. Wang *et al.*, "Power electronics building block (PEBB) design based on 1.7 kV SiC MOSFET modules," in *Proc. IEEE Electric Ship Technol. Symp.*, 2017, pp. 612–619.

[15] D. Maksimovic, A. Stankovic, V. Thottuvelil, and G. Verghese, "Modeling and simulation of power electronic converters," *Proc. IEEE*, vol. 89, no. 6, pp. 898–912, Jun. 2001.

[16] N. Femia and G. Spagnuolo, "True worst-case circuit tolerance analysis using genetic algorithms and affine arithmetic," *IEEE Trans. Circuits Syst. I, Fundam. Theory Appl.*, vol. 47, no. 9, pp. 1285–1296, Sep. 2000.

[17] R. White, "An introduction to six sigma with a design example," in *Proc. Appl. Power Electron. Conf. Expo.*, 1992, pp. 28–35.

[18] N. R. Mehrabadi, R. Burgos, C. Roy, and D. Boroyevich, "Power electronics modeling and design: Using parametric and model-form uncertainty quantification to assess predictive accuracy of power converter models," *IEEE Power Electron. Mag.*, vol. 4, no. 4, pp. 44–52, Dec. 2017.

[19] D. G. Holmes and B. P. McGrath, "Opportunities for harmonic cancellation with carrier-based PWM for a two-level and multilevel cascaded inverters," *IEEE Trans. Ind. Appl.*, vol. 37, no. 2, pp. 574–582, Mar./Apr. 2001.

[20] B. Li, R. Yang, D. Xu, G. Wang, W. Wang, and D. Xu, "Analysis of the phase-shifted carrier modulation for modular multilevel converters," *IEEE Trans. Power Electron.*, vol. 30, no. 1, pp. 297–310, Jan. 2015.

[21] M. Hagiwara and H. Akagi, "PWM control and experiment of modular multilevel converter," in *Proc. IEEE Power Electron. Spec. Conf.*, 2008, pp. 154–161.

[22] X. She, A. Huang, X. Ni, and R. Burgos, "AC circulating currents suppression in modular multilevel converter," in *Proc. 38th Annu. Conf. IEEE Ind. Electron. Soc.*, 2012, pp. 191–196.

[23] N. Rashidi Mehrabadi, B. Wen, R. Burgos, D. Boroyevich, and C. Roy, "Verification, validation and uncertainty quantification (VV\&UQ) framework applicable to power electronics systems," *SAE Tech. Paper*, vol. 1, no. 2176, 2014.

[24] C. J. Roy and W. L. Oberkampf, "A comprehensive framework for verification, validation, and uncertainty quantification in scientific computing," *Comput. Methods Appl. Mech. Eng.*, vol. 200, no. 25, pp. 2131–2144, 2011.

[25] D. L. Donoho, "High-dimensional data analysis: The curses and blessings of dimensionality," *AMS Math Challenges Lecture*, vol. 1, no. 2000, p. 32, 2000.

[26] I. M. Sobol, "Global sensitivity indices for nonlinear mathematical models and their Monte Carlo estimates," *Math. Comput. Simul.*, vol. 55, no. 1–3, pp. 271–280, 2001.

[27] A. Saltelli, P. Annoni, I. Azzini, F. Campolongo, M. Ratto, and S. Tarantola, "Variance based sensitivity analysis of model output. design and estimator for the total sensitivity index," *Comput. Phys. Commun.*, vol. 181, no. 2, pp. 259–270, 2010.

[28] I. Voyles and C. Roy, "Evaluation of model validation techniques in the presence of aleatory and epistemic input uncertainties," AIAA Paper 2015-1374, 2015.

[29] M. Hagiwara, K. Nishimura, and H. Akagi, "A medium-voltage motor drive with a modular multilevel PWM inverter," *IEEE Trans. Power Electron.*, vol. 25, no. 7, pp. 1786–1799, Jul. 2010.

[30] M. Davies, M. Dommaschk, J. Dorn, J. Lang, D. Retzmann, and D. Soerangr, "HVDC plus–basics and principle of operation," in *Proc. Special Edition Cigré Expo.*, 2008.

[31] M. Jakšić *et al.*, "Medium-voltage impedance measurement unit for assessing the system stability of electric ships," *IEEE Trans. Energy Convers.*, vol. 32, no. 2, pp. 829–841, Jun. 2017.

[32] G. D. Wyss and K. H. Jorgensen, *A User's Guide to LHS: Sandia's Latin Hypercube Sampling Software*. SAND98-0210, Albuquerque, NM, USA: Sandia Nat. Lab., 1998.

[33] J. Yu, R. Burgos, N. R. Mehrabadi, and D. Boroyevich. "Design of a SiC-based modular multilevel converter for medium voltage DC distriution system," in *Proc. IEEE Appl. Power Electron. Conf. Expo.*, 2017, pp. 467–473.

[34] D. C. Montgomery, E. A. Peck, and G. G. Vining, *Introduction to Linear Regression Analysis*. Hoboken, NJ, USA: Wiley, 2012.

[35] D. C. Montgomery, *Design and Analysis of Experiments*. Hoboken, NJ, USA: Wiley, 2017.

[36] D. J. MacKay, "Introduction to Gaussian processes," *NATO ASI Series F Comput. Syst. Sci.*, vol. 168, pp. 133–166, 1998.

[37] C. E. Rasmussen and C. K. Williams, *Gaussian Processes for Machine Learning*, vol. 1. Cambridge, MA, USA: MIT Press, 2006.

Niloofar Rashidi (Member, IEEE) received the B.S. degree in electrical engineering from the Amirkabir University of Technology, Tehran, Iran, in 2012, and the M.S. degree in electrical engineering, the M.A. degree in data analysis and applied statistics, and the Ph.D. degree in electrical engineering from the Virginia Polytechnic Institute and State University, Blacksburg, VA, USA, in 2014, 2017, and 2018, respectively.

From 2012 to 2018, she was a Research Assistant with the Center for Power Electronics Systems, Virginia Polytechnic Institute and State University. She is currently a Hardware Engineer with Apple Inc., Cupertino, CA, USA. Her research interests include modeling and design optimization of power electronics converters and systems and design under uncertainty.

Dr. Rashidi is a member of the IEEE Power Electronics Society, IEEE Industry Applications Society, and ASME.

Rolando Burgos (Member, IEEE) received the B.S. degree in electronics engineering, the Electronics Engineering Professional degree, and the M.S. and Ph.D. degrees in electrical engineering from the University of Concepción, Concepción, Chile, in 1995, 1997, 1999, and 2002, respectively.

In 2002, he joined as a Postdoctoral Fellow with the Center for Power Electronics Systems (CPES), Virginia Tech, Blacksburg, VA, USA, where he became the Research Scientist in 2003, and Research Assistant Professor in 2005. In 2009, he joined ABB Corporate Research in Raleigh, NC, where he was a Scientist from 2009 to 2010, and Principal Scientist from 2010 to 2012. In 2010, he was appointed as an Adjunct Associate Professor with the Electrical and Computer Engineering Department, North Carolina State University, the Future Renewable Electric Energy Delivery and Management (FREEDM) Systems Center. In 2012, he returned to Virginia Tech, as an Associate Professor, with The Bradley Department of Electrical and Computer Engineering, where he has been a Professor and member of the CPES Executive Board since 2019. His research interests include high power density wide-bandgap semiconductor-based power conversion in low-voltage and medium-voltage applications, packaging and integration, electromagnetic interference and electromagnetic compatibility, multiphase multilevel power converters, modeling and control, grid power electronics systems, and the stability of ac and dc power systems.

Dr. Burgos is a member of the IEEE Power Electronics Society, where he currently serves as the Chair of the Technical Committee on Power and Control Core Technologies. He also serves as an Associate Editor of the IEEE TRANSACTIONS ON POWER ELECTRONICS, and the IEEE JOURNAL OF EMERGING AND SELECTED TOPICS IN POWER ELECTRONICS. He is a member of the IEEE Industry Applications Society, the IEEE Industrial Electronics Society, and the IEEE Power and Energy Society.

Chris Roy received the undergraduate degree in mechanical engineering from Duke University, Durham, NC, USA, in 1992, the master's degree in aerospace engineering from Texas A&M University, Texas, TX, USA, in 1994, and the Doctorate degree in aerospace engineering from North Carolina State University, Raleigh, NC, USA, in 1998.

After spending 5 years as a Senior Member of the Technical Staff with Sandia National Laboratories in Albuquerque, NM, USA, he moved to academia and is currently a Full Professor with the Crofton Department of Aerospace and Ocean Engineering, Virginia Tech. He has authored or coauthored more than 180 books, book chapters, journal articles, and conference papers in the areas of computational fluid dynamics, verification, validation, and uncertainty quantification. He has coauthored the book *Verification and Validation in Scientific Computing* (Cambridge University Press, 2010).

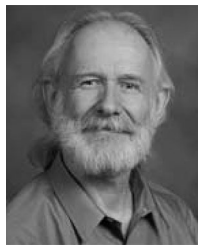

Dushan Boroyevich (Fellow, IEEE) received the Dipl.Ing. degree from the University of Belgrade, Belgrade, Serbia, in 1976, and the M.S. degree from the University of Novi Sad, Novi Sad, Serbia (then Yogoslavia), in 1982, and the Ph.D. degree from the Virginia Polytechnic Institute and State University (Virginia Tech), Blacksburg, VA, USA, in 1986.

From 1986 to 1990, he was an Assistant Professor and Director of the Power and Industrial Electronics Research Program with the Institute for Power and Electronic Engineering, the University of Novi Sad. He then joined the Bradley Department of Electrical and Computer Engineering, Virginia Tech, as an Associate Professor. He is currently the University Distinguished Professor with the Department and Director of the Center for Power Electronics Systems. From 2011 to 2012, he was the President of the IEEE Power Electronics Society. His research interests include electronic power distribution systems, multi-phase power conversion, power electronics systems modeling and control, and integrated design of power converters.

Dr. Boroyevich is a member of the US National Academy of Engineering and recipient of numerous awards, including the IEEE William E. Newell Power Electronics Technical Field Award, and the European Power Electronics Association Outstanding Achievement Award.